A Study of a Cavity Nearby a Pulsar at -60º Latitude in the Far Infrared Map

A. K. Jha and B. Aryal

Journal of Nepal Physical Society

Volume 4, Issue 1, February 2017

ISSN: 2392-473X

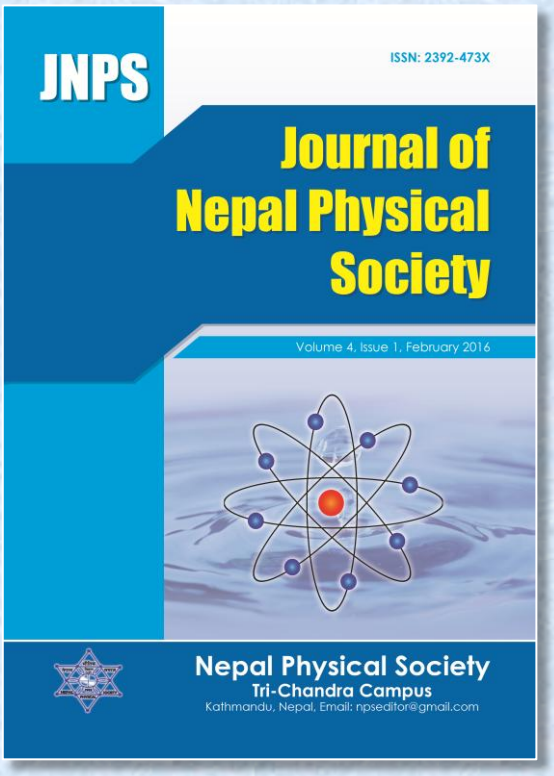

JNPS, **4** (1), 33-41 (2017)

Published by:

Nepal Physical Society

P.O. Box : 2934

Tri-Chandra Campus

Kathmandu, Nepal

Email: npseditor@gmail.com

JNPS ***4*** *(1), 33-41 (2017)*
ISSN: 2392-473X

Research Article

A Study of a Cavity Nearby a Pulsar at -60º Latitude in the Far Infrared Map

A. K. Jha[*] and B. Aryal
Central Department of Physics, Tribhuvan University, Kirtipur, Nepal
[*]*Corresponding Email: astroajay123@gmail.com*

ABSTRACT

We present physical properties of a region in the interstellar medium where the past evolutionary remnant of pulsar evolution is observed. For this, a systematic search of dust structure in the far infrared (100 µm and 60 µm) IRAS (Infrared Astronomical Satellite) survey was performed using Sky View Observatory. Our selection criteria are as follows: (a) Cavity should be greater than 0.25 degree in diameter and (b) the cavity should have 3-fold minima in flux density. In the 100 micron infrared map, a new cavity-like isolated far infrared dust structure (size ~ 1.62 pc x 0.98 pc) is found at R.A. (J2000) 18^h 33^m 14.8^s and Dec. (J2000) -60^0 $23^{'}$ $24^{''}$. We have studied flux density variation and temperature variation within the structure. We found that the dust color temperature varies from 22.78 K to 24.78 K, with offset of 2 K. The dust mass of each pixel of the region of interest was calculated using their dust color temperature. The excess mass in the region was found to be 1.62 x 10^{23} Kg. The energy required to create that inhomogeneity in the structure is calculated to be 3.24 x10^{35} J.

Keywords: Interstellar medium, Inhomogeinity in ISM, Pulsar wind.

INTRODUCTION

Massive stars (8-25 M) ends its life in a supernova, this event produces supernova remnants with rapidly rotating neutron star. In other words, massive star explodes in supernova and center of star collapse to form neutron star. Materials (stellar debris) around it move away with very high rate of speed. This event not only produces a disturbance in interstellar medium (ISM) but in other hand it has enriched the medium with material heavier than hydrogen and helium (Karttunen *et al.*, 2007).

Because of conservation of angular momentum neutron star spins very rapidly, there is magnetic field that was in the original star that gets compressed and gets frozen into that surface of neutron star, now have strong spin magnet basically in space. The charge particle of Neutron star move at relativistic speed varying the speed of light and that cause sorts of radiation be generated. Radio waves come out of the magnetic poles of neutron stars and because they are spinning and magnetic axis don't happen to be align to rotation axis just like our earth, if these radio beams happen to pass by earth through our line of sight we see pulse of radio wave. So, because of these sweeping of light house type beam across our line of sight we see pulses of radiation that's why we called them pulsars (Bhattacharya *et al.*, 2008).

Hence, Pulsars are rotating neutron star in which co-rotating magnetic field (~10^{12} G) can accelerate charge particle to the cosmic ray energies. These rapidly rotating neutron stars have been proposed as the energy source in supernova remnant (Wheeler and Pacini, 1966). Further in 1968, Gold and Pacini have suggested that pulsars are rotating magnetic neutron stars formed in supernova explosion. Interestingly, not only they formed there, they ejected out after the explosion dashing away envelop of supernova remnant at the speed of 100-1000 Km/Sec (Pacini, 1967).

Pulsar moves through either ISM or in more interestingly in supernova remnant. In both cases, there exists a three folds structure consisting of the wind. These three fold structures are i) Terminating Shock, ii) Contact Discontinuity, & iii) Bow Shock (Budhathoki, 2015).

Pulsar winds are composed of charged particles accelerated to relativistic speed by the rapidly rotating, super strong magnetic field of the spinning pulsar. The pulsar wind streams in the ISM, creating a standing shock wave, where it is decelerated to sub-relativistic speed. As, Pulsars are thought to eject relativistic moving charge particles

that energies the surrounding medium with the formation of Pulsar Wind and thus formed a Pulsar wind driven structure in ISM (Becker, 2009).

The pulsar wind driven structure also known as cavity is the very low temperature and mass region so we need that spectrum through which the region become more visible and we can get more information which is actually the region of Infrared from electromagnetic spectrum. In cavity we studied old and very cold dusts that are totally opaque in the optical but bright in the Infrared Region. There are many space telescopes studying in Infrared Region. We took data provided by IRAS (Infrared Astronomical Satellite). Almost the entire sky was covered in four pass bands (12, 25, 60 and 100 microns). Although the IRAS mission took place two decades ago – the maps are still not exhausted of their riches which is the one reason that motivates us to carry our study in IRAS map and discovered the cavity structure around pulsar (Beichman *et al.*, 1988).

REGION OF INTEREST

Sky view Virtual Observatory (http://skyview.gsfc.nasa.gov/current/cgi/query.pl) was used in order to search a deep cavity structure for different wavelength IRAS bands. We carried a systematic search of IRAS maps available in the Sky view Virtual Observatory. Sky view is intended as a quick look facility to see our sky in different spectrum. The core of Sky view is a geometry engine which enables the transformation of the data from existing surveys into the image we have requested. In this course we downloaded the JPEG image of about 100 pulsars and we took some image for the further study. Out of the selected candidates, we selected one image for systematic research by finding the work that has been done on the objects near to our candidate with the help of SIMBAD (http://simbad.u-strasbg.fr/simbad/).

In the process of scanning the sky covering the range of J2000 coordinate system provided by K. W. Suh and Y. J. Kwon (2011), we found some interesting isolated structures surrounding planetary nebula, pulsars, white dwarfs and different galaxies. We entered 100 Pulsar coordinates out of 1428 given from catalog in terms of R.A. (hour, min, sec) and Dec (degree, min, sec) and downloaded 800 different images in JPEG format (200 images each in four different bands of IRAS; 12 µm, 25 µm, 60 µm and 100 µm) (Suh *et al.*, 2009).

Out of the 800 sky view image the structure located around the pulsar J1833-6023 was selected. The selections of the region are justified by the following reasons:

- The structure is seen to be isolated cavity.
- Around the cavity, the collection of expelled mass due to pulsar activity is seen clearly in 100 µm and 60 µm which suggest that the region of cavity is very cold due to lack of interstellar cloud.

The most important thing is that this structure is not yet studied. We have reviewed the ADS and found that only the catalogs are available for the point sources. Thus, this structure is not yet studied. We intend to study the physical properties of this structure.

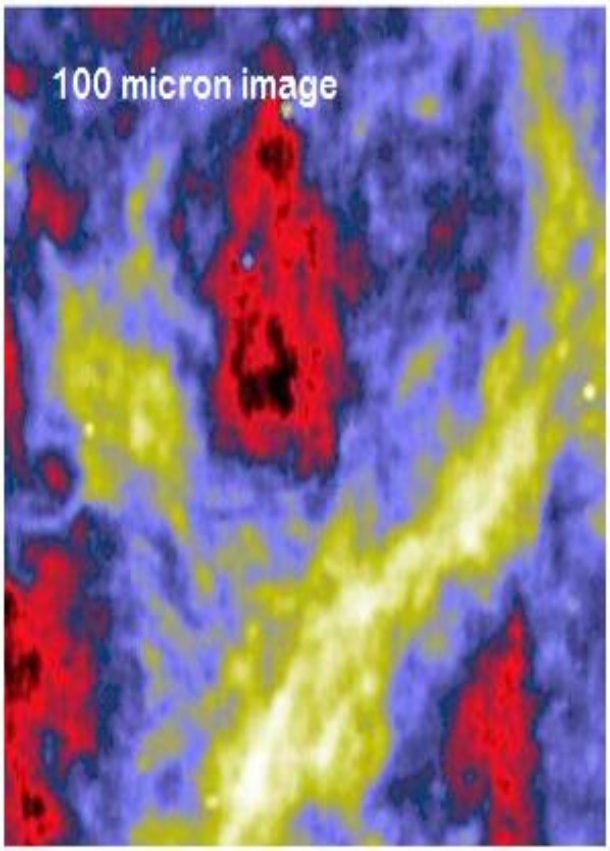

Fig. 1. Best 5^0x 5^0 pixel size selected Region of interest where the cavity is seen prominently. (Web)

The IRAS image at 100 µm and 60 µm of the selected candidate pulsar are shown in figure 2.

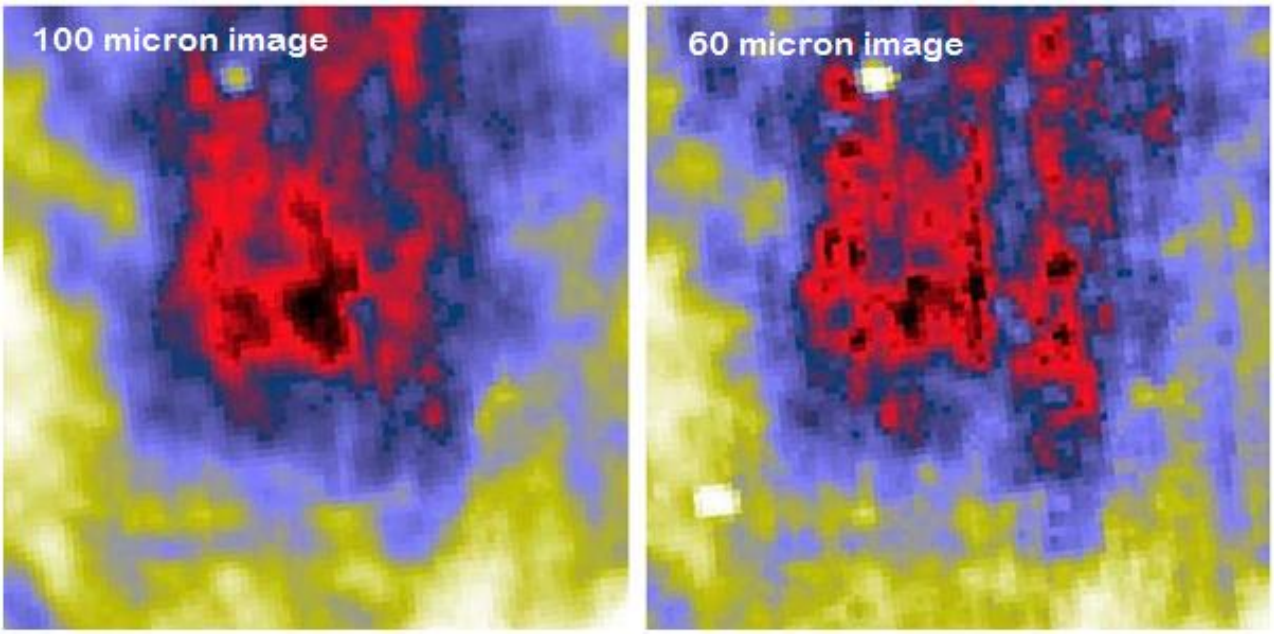

Fig. 2. Selected candidate of size 2^0x 2^0 IRAS jpeg images 100μm (left) & 60μm (right). (Web)

Also SIMBAD was used to find the degree of study made on these individual cavity structures. We found that structure found in Galactic longitude 278.25^0 and Galactic latitude 59.62^0 was less studied and hence making it more appropriate for our study.

METHODS

We adopt the following methods to find the size, dust color temperature and dust mass of the structure. In addition, we calculated the excess mass and the energy of the pulsar wind needed to expel the excess mass.

Dust Color Temperature Estimation

The dust color temperature from the IRAS 60 micron and 100 micron flux densities was calculated. The temperature is determined by the ratio of the 60 micron and 100 micron flux densities (Schnee *et al.*, 2005). The dust temperature T_d in each pixel of a FITS image can be obtained by assuming that the dust in a single beam is isothermal and that the observed ratio of 60 micron to 100 micron emission is due to black body radiation from dust grains at Td, modified by a power law emissivity spectral index. The flux density F_i of emission at a wavelength λ_i , is given by,

$$F_i = \left[\frac{2hc}{\lambda_i^3\left(e^{\frac{hc}{\lambda_i KT_d}}-1\right)}\right] N_d \alpha \lambda_i^{-\beta} \Omega_i \qquad (1)$$

Where, N_d represents column density of dust grains, α is a constant that relates the flux to the optical depth of the dust, β is the emissivity spectral index, and Ω_i is the solid angle subtended at λ_i by the detector. Following Dupac *et al.* (2003), we use the equation,

$$\beta = \frac{1}{\delta+\omega T_d} \qquad (2)$$

to describe the observed inverse relationship between temperature and emissivity spectral index. With the assumptions that the dust emission is optically thin at 60 micron and 100 micron and that $\Omega_{60} \approx \Omega_{100}$ (true for IRAS image), we can write the ratio, R, of the flux densities at 60 micron and 100 micron as

$$R = 0.6^{-(3+\beta)} \frac{e^{\frac{144}{T_d}}-1}{e^{\frac{240}{T_d}}-1} \qquad (3)$$

For a smaller value of T_d, 1 can be dropped from both numerator and denominator of equation 3 and it takes the form

$$R = 0.6^{-(3+\beta)} e^{\frac{144}{T_d}-\frac{240}{T_d}} \qquad (4)$$

Taking natural logarithm on both sides of equation 4, we find the expression for the temperature as

$$T_d = -96 \frac{1}{ln\{R \times 0.6^{(3+\beta)}\}} \qquad (5)$$

The value of the spectral emissivity index (β) depends on dust grain properties as composition, size, and compactness. For reference, a pure blackbody would have β = 0, the amorphous layer-lattice matter has β ~1, and the metals and crystalline dielectrics have $\beta \sim 2$. (Dupac *et al.*, 2003).

Where R is given by

$$R = \frac{F(60\ \mu m)}{F(100\ \mu m)} \quad (6)$$

F(60 micron) and F(100 micron) are the flux densities at $60\ \mu$m and $100\ \mu$m, respectively. In this way we can use equation (1) for the determination of the dust grain temperature (Dupac *et al.*, 2003).

Dust Mass Estimation

The dust masses are estimated from the IR flux densities. The resulting dust mass depends on the physical and chemical properties of the dust grains, the adopted dust temperature T_d and the distance D to the object (Hildebrand, 1983).

$$M_{dust} = \frac{4}{3}\frac{a\rho}{Q_\nu}\left[\frac{S_\nu D^2}{B(\nu,T)}\right] \quad (7)$$

Where,

a = Weighted grain size = 0.1 μm

ρ = Grain density = $3000 Kg\ m^{-3}$

Q_ν= grain emissivity = 0 .0010 for 100μm and 0.0046 for 60μm respectively (Young et al. 1993)

S_ν= total flux density of the region whose mass is to be determined

$S_\nu = f \times 5.288 \times 10^{-9}\ MJy/Sr$

D = distance of the structure

$B(\nu,T)$ = Planck's function (Beichman et al. 1988).

$$B(\nu,T) = \frac{2h\nu^3}{c^2}\left[\frac{1}{e^{\frac{h\nu}{kT}}-1}\right] \quad (8)$$

Where,

h = Planck's constant

c = velocity of light

ν = frequency at which the emission is observed

T = the average temperatures of the region.

Values of different parameters we use in the calculation of the dust mass in our interest are as follows:

Using these values the equation (3) takes the form (Hildebrand 1983):

$$M_{dust} = 0.4\left[\frac{S_\nu D^2}{B(\nu,T)}\right] \quad (9)$$

We use the equation 5 for the calculation of the dust mass. It is clear from the expression (4) that the value of Planck function $B(\nu,T)$ for longer wavelength is higher than that of the shorter wavelength. Consequently, the range of $B(\nu,T)$ for fixed temperature (say ΔT) goes narrower if wavelength of the images increases (Beichman *et al.*, 1988).

Energy Estimation

To estimate the energy of the region of the interest we assume here that our targeted energy values are those with this energy value mass of central region moving outward. The outer wind expands quietly at a certain velocity (Johnston *et al.*, 2001). This is by far the largest part of the wind (extending up to 1000 - 100000 R_* depending on the mass-loss history) with temperatures decreasing to ~10 K. Chemically, the outer wind remains quite active with interstellar UV photons photo dissociating molecules. The photo dissociation products can trigger subsequent molecule formation through neutral-neutral and ion-molecule reactions. We use calculated value of average mass deficit per pixel. With the help of classical kinetic energy relation we are focused to estimate the values of outflow energy.

$$E = \frac{1}{2}M_{deficit}u_{out}^2 \quad (10)$$

RESULTS AND DISCUSSION

Contour Map

We intend to study the cavity structure at 60 μm and 100 μm. We adopt the method of drawing contours at different levels so that we can separate the region of maximum and minimum flux density. The numbers of the contours are according to the requirements so as to include the maximum features of the region. The number of the contour in 100 μm and 60 μm fits image are chosen independently to make the best contour level. The contour for 100 μm and 60 μm picture are shown in Fig.3. We are interested in these minima to study the flux density within the region because we concern our focus on temperature profile and the mass distribution of the dust within the isolated structure in each pixel to estimate the energy of pulsar at the center of the cavity at the time of formation of cavity. While going through the systematic search we found an isolated cavity in the interstellar medium in the region around the pulsar `J1833-6023', having faint emission in all four band of infrared in the IRAS survey. With the help of software ALADIN7.5, we have drawn contour maps to distinguish the regions with minimum flux in the region of interest. In figure 3 three contours corresponding to the levels 13, 8 and 1 are constructed using ALADIN7.5.

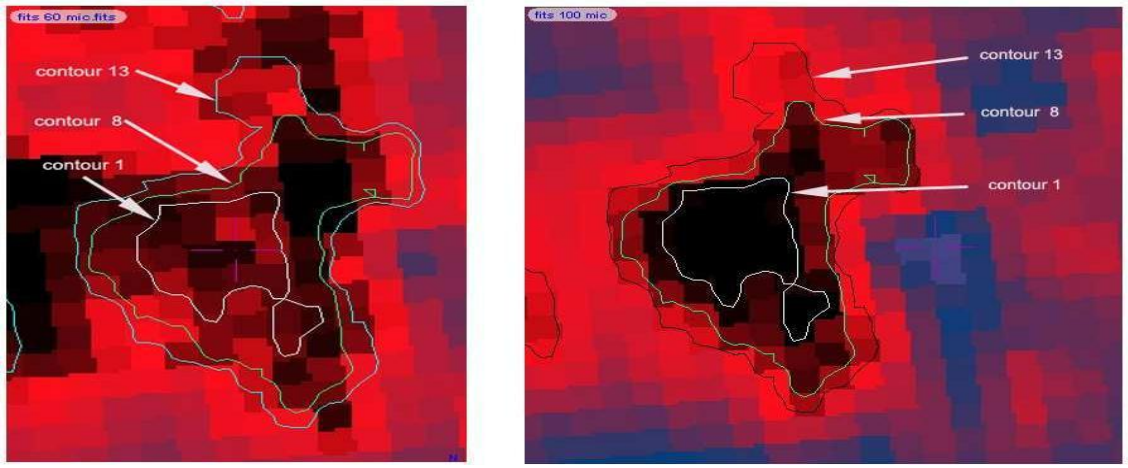

Fig. 3. Showing contour levels in fits image of 60μm (left) and 100μm (right). Three contours are in 100μm image and three contours in 60 μm image for the best selection of contour.

Flux Density Variation

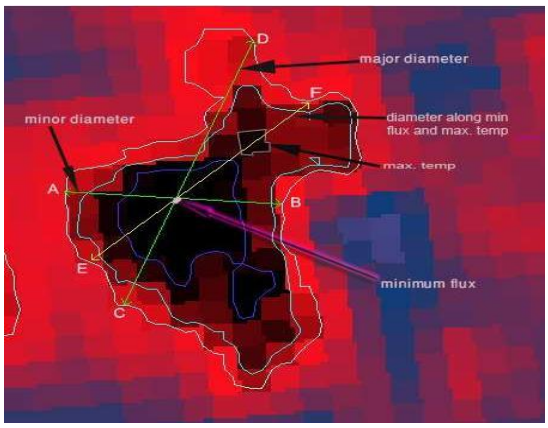

Fig. 4. Figure showing minor axis (AB), major axis (CD) and line joining the maximum temperature region and minimum flux region (EF), while studying the flux variation in the field of view of 100 μm FITS image.

By using the ALADIN7.5 software, flux density variation of the region of interest is studied. We obtained the graph of flux density variation along the major axis, minor axis and line joining the maximum temperature region and minimum flux region. Figure 4 shows the major axis, minor axis and line joining the maximum temperature region and minimum flux region.

The Flux density variation with distance along major diameter is shown in figure 5.

The equation representing the second degree parabola for major diameter is

$$F = 3.91 - 0.04\mathrm{d} + 0.03 \times 10^{-1}\mathrm{d}^2 \qquad (11)$$

The best fit polynomial (fifth degree polynomial) is given by;

$$F = 4.04 - 0.02\mathrm{d} - 0.04\mathrm{d}^2 + 0.09 \times 10^{-1}\mathrm{d}^3 - 0.06 \times 10^{-2}\mathrm{d}^4 + 0.01 \times 10^{-3}\mathrm{d}^5 \qquad (12)$$

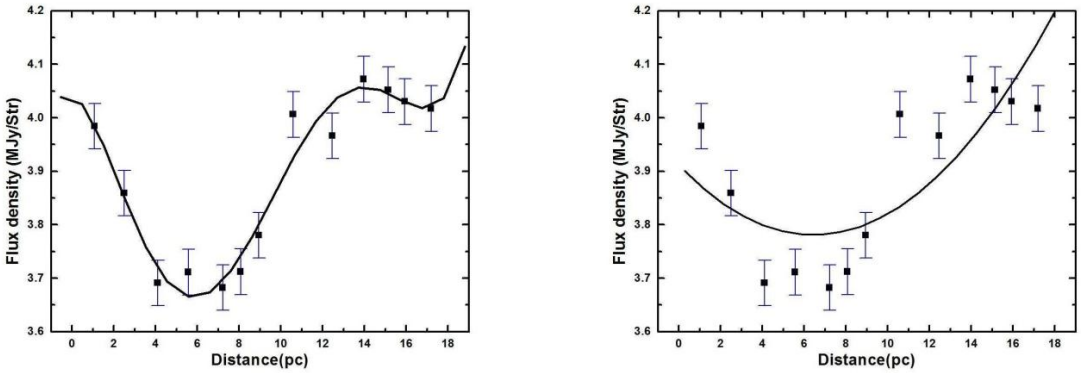

Fig. 5. The distribution of flux density along major diameter; the first graph (left) represents the best fit fifth degree polynomial and the second graph(right) represents second degree polynomial. The solid squares with $\pm\sigma/\sqrt{n}$ error bars represent the standard error of the distribution.

The Gaussian distribution represents the natural process without any external effect. As we know that the lines form of the Gaussian equation (after taking logarithm) is second order polynomial without constant slope. Equation 11 represents second order polynomial with a small (-0.04) constant slope. Thus, a deviation from Gaussian distribution is noticed but this deviation is not very strong. For best fit, we choose the fifth order polynomial because the standard error is minimum at fifth order. Equation 12 is the fifth order polynomial having smaller constant slope (-0.02) than the second order polynomial, suggesting a closeness between the Gaussian distribution. The deviation is because of the effect of pulsar wind.

Hence, it seems that the flux density variation along major diameter is disturbed from the pulsar wind. The flux density variation with distance along minor diameter is shown in figure 5.4 given below.

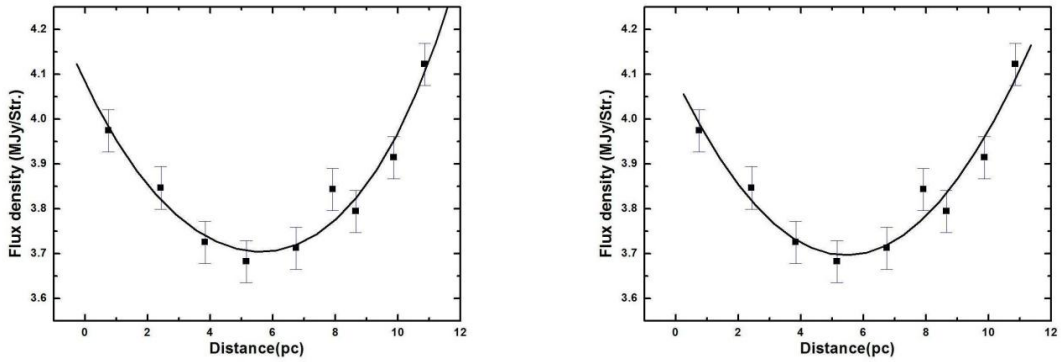

Fig. 6. The distribution of flux density along minor diameter; the first graph (left) represents the best fit fourth order polynomial and second graph (right) represents second degree polynomial. The solid squares with $\pm {}^{\sigma}/_{\sqrt{n}}$ error bars represent the standard error of the distribution.

The equation representing the second degree parabola for minor diameter is given by;

$$F = 4.09 - 0.14\mathrm{d} + 0.01\mathrm{d}^2 \quad (13)$$

The best fit polynomial of fifth order is,

$$F = 4.08 - 0.15\mathrm{d} + 0.02\mathrm{d}^2 - 0.01 \times 10^{-1}\mathrm{d}^3 + 0.06 \times 10^{-3}\mathrm{d}^4 \quad (14)$$

From the figure 6, we can see that there is smooth variation of the flux along the minor diameter. The flux decreases slowly with distance to reach the minima point and symmetrically increase to maximum value. Along the line of minor diameter, we can see that the changing slope is larger and it doesn't change significantly even changing slope is growing. This suggests that the distribution of flux density along minor diameter is also deviated from expected Gaussian distribution but not as strong as the major diameter.

For the detailed calculation, we pointed the location of high temperature region and draw a line joining the point of high temperature and low flux (minima). The flux density variation with distance along minimum flux and maximum temperature is shown in figure given below.

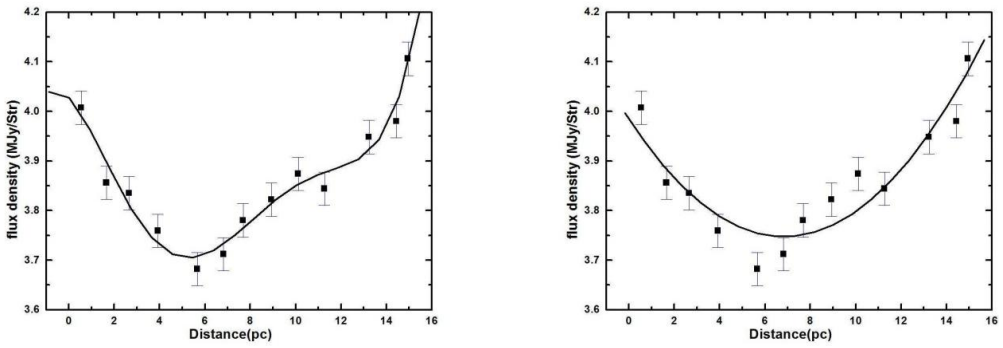

Fig. 7. The distribution of flux density along minimum flux and maximum temperature; the first graph represents the best fit fifth order polynomial and second graph represents second degree polynomial. The solid square with $\pm \frac{\sigma}{\sqrt{n}}$ error bars represent the standard error of the distribution.

The equation representing the second degree parabola is given by;

$$F = 3.98 - 0.06\mathrm{d} + 0.05 \times 10^{-1}\mathrm{d}^2 \quad (15)$$

The best fit polynomial is of fifth order;

$$F = 4.03 - 0.05\mathrm{d} - 0.03\mathrm{d}^2 + 0.008 \times 10^{-1}\mathrm{d}^3 + 0.08 \times 10^{-2}\mathrm{d}^4 + 0.02 \times 10^{-3}\mathrm{d}^5 \quad (16)$$

From equations (15) & (16) i.e., the line along minimum flux and maximum temperature, we can see that flux density is deviated less from expected Gaussian distribution but significant than that of major diameter.

Dust Color Temperature

We calculated dust color temperature of each pixel inside minima lying in the region of interest. For the calculation of temperature we choose the value of β = 2 (Dupac et al. 2003) . The region with maximum and minimum temperature is found to lie in the range of 24.78 K to 22.78 K. An offset of the difference suggests the in influence of magnetic field around the region of interest and thus our structure is not independently evolved. If this value is less than 2 K, this structure is less disturbed from the Pulsar wind and its radiation. If it is more, the effect of pulsar wind cannot be ruled out. In our case, we found that the difference between minimum and maximum temperature is about 2 K. The average temperature of the dust in region of our interest is calculated to be 23.78 K.

Dust Mass

The dust color temperature, flux density and the distance is used to estimate dust mass using 100 μm IRAS image. The infrared flux is obtained from Groningen IRAS server available at official website of Sky View virtual observatory. By using the average of the maximum and minimum temperature of each maxima summing up of the flux density of each pixel inside the region, the value of average temperature and the total flux density for all the maxima can be known. For the calculation of the mass we need the distance to the region of interest. The distance of the selected region is estimated to be 310 pc by color-magnitude method.

We calculated the mass of the structure enclosed by each contour. The separate mass of the structure enclosed by the each contour is tabulated below:

Table 1. The table shows the mass of each contour. First column shows the contour level, second column shows the dust mass of corresponding contour, third column shows dust mass of corresponding contour in terms of solar mass and fourth column shows ratio of dust mass of contour in terms of contour - 1 (lower), having lowest mass.

Contour Level	Mass (kg)	Mass (M_o)	Mass ratio
inner contour	1.28×10^{26}	0.639×10^{-4}	1
mid contour	2.65×10^{26}	0.132×10^{-3}	2.069
outer contour	2.827×10^{26}	0.141×10^{-3}	2.209

Calculation of Excess Mass

For the calculation of excess mass, we drew two concentric circles having diameter equal to the diameter of major axis called big circle and another having diameter equal to minor axis called small circle. Systematically, here we calculated the dust color mass inside the big as well as small circle and their difference. And the mass difference was divided by the number of pixel present inside the big circle to calculate the average. The average value of dust color mass was multiplied with the total number of pixel inside the small circle which is the projected mass of small circle. Finally we calculated the difference of real and projected mass of the small circle and its average too. The circle was drawn using the ALADIN7.5 as in figure 8.

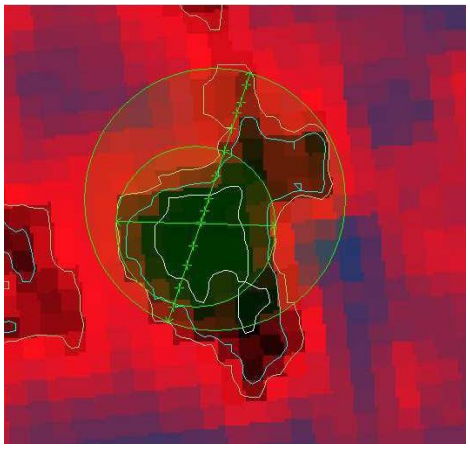

Fig. 8. Figure of excess mass. The outer circle (big) and inner circle (small) has diameter as major axis and minor axis respectively.

Mass deficit per pixel in inner circle is found to be 1.62×10^{23} Kg.

The systematic calculation of excess mass and the average mass of each pixel calculated to be in the range of ~10^{23}Kg. It revealed that the system is not very compact as it has low mass.

Size of the Structure

To measure the major and minor diameter for the outer contour level, we use a simple ex-pression for the calculation. L = R$\times \theta$, where R = 310 pc and θ = pixel size (in radian). The diameters of the structure are tabulated below.

Table 2. The table shows major and minor diameter of the cavity in the 100μm image.

Major diameter (pc)	Minor diameter (pc)
1.62	0.98

Thus, the size of the structure is 1.62 pc × 0.98 pc.

Energy Estimation

The mass deficit is found to be 1.62×10^{23}Kg. Using this value and the velocity of pulsar wind 2000 Km/s (Johnston *et al.*, 2001) the energy of pulsar wind energy is calculated to be 3.24×10^{35} J.

CONCLUSION

We have carried out a systematic search of cavity structure in the far infrared (100 μm and 60 μm) IRAS (Infrared Astronomical Satellite) survey. We found a pulsar pumped cavity at galactic longitude 278.25^0 and latitude -59.62^0 which was scanned for pixel size 2^0x 2^0 field of view at 100μm and 60μm IRAS image. The distance of the structure was found to be about 310pc.The physical property of the structure, a study of flux density variation, dust color temperature, excess mass and the energy of the pulsar to create such cavity in ISM are studied.

The size of the cavity structure is found to be about 1.62 pc × 0.98 pc. Where, major and minor diameter is found to be 1.62 pc and 0.98 pc respectively. The maximum flux region is found to be located at the lower part of outer contour region, at R.A.(J2000) = $18^h34^m47{:}44^s$, Dec.(J2000) = $-60^0\ 15'00.6''$.The minimum flux region is found to be located at center of inner contour region, at R.A.(J2000) = $18^h34^m55.98^s$, Dec.(J2000) = $-60^0\ 05'59.3''$.A study of flux density variation shows a prominent cavity structure at 100μm image and distribution of flux density variation along major diameter of the structure shows that it is deviated from Gaussian distribution which may be due to pulsar wind for the formation of that cavity where as on minor diameter it is not so prominent. In addition, similar deviation from Gaussian distribution is found along line joining the minimum flux and the maximum temperature region. Gaussian-like distribution suggests that the cavity structure is isolated and less disturbed from the external factors. The dust color temperature is found to lie in the range 22.78 K to 24.78 K, with an offset of about 2 K. This temperature range suggests that cavity is not evolved independently. The mass deficit per pixel is found to be $1.62x10^{23}$ Kg. The total mass of the dust in the structure is found about $6.755x\ 10^{26}$ Kg. The energy of the pulsar to expel the excess mass was found to be $3.24\ x\ 10^{35}$ J.

ACKNOWLEDGEMENT

We acknowledge Prof. Dr. Ronald Weinberger of Innsbruck University, Austria for his comments to revise this article. We thank Mr. Himal Acharya, Ms. Nisha Budhathoki and Mr. Sujit Kumar Thakur for their help during preliminary data processing. One of us AKJ acknowledge Central Department of Physics, Tribhuvan University, Nepal for necessary supports.

REFERENCES

Becker, W. (2009). Neutron Stars and Pulsars, Springer, pp. 213.

Beichman, C. A.; Neugebauer, G.; Habing, H. J.; Clegg, P. E.; Chester, T. J. (1988). Infrared Astronomical Satellite (IRAS) Catalogues and Atlases I: Explanatory Supplement. US Government Printing Office, Washington.

Bhattacharya, A. A.; Joardar, S. & Bhattacharya, R. (2008). Astronomy & Astrophysics, Infinity Science Press, India.

Budhathoki, N. (2015). M. Sc. Physics Dissertation, Central Department of Physics, T. U.

Dupac, X.; Bernard, J. P.; Boudet, N.; Giard, M.; Lamarre, J. M.; Mny, C. et al. (2003). *A&A* **404:** L11.

Hildebrand, R. H. (1983). *QJRAS*, **24**: 267.

http://simbad.u-strasbg.fr/simbad/ (SIMBAD, 2015)

http://skyview.gsfc.nasa.gov/current/cgi/query.pl (July.2015)

Johnston, S.; Wex, N.; Nicastro, L.; Manchester, N.; Lyne, A. G. *The 1997 periastron.*

Karttunen H.; Krooger, P.; Oja, H.; Poutanen, M.; Donner, K. J. (2007). Fundamental Astronomy, 5th edition, Springer Berlin Heidelberg, USA.

Pacini, F. (1967). *Nature*, **216**: 567.

Passage of the binary pulsar PSR B1259-63, p.4, (2001)

Schnee S. L.; Ridge N. A.; Goodman, A. A.; Jason, G. L. (2005). *APJ*, **634**: 442.

Suh, K. W., and Kwon, Y. J. (2009). *JKAS*, **42**: 81.

Young, K.; Phillips, T. G.; Knaap, G. R. (1993). *APJ*, **409**: 725.